

Many-Body Localization in Translational Invariant Diamond Ladders with Flat Bands

Mirko Daumann,¹ Robin Steinigeweg,² and Thomas Dahm^{1,*}

¹Fakultät für Physik, Universität Bielefeld, Postfach 100131, D-33501 Bielefeld, Germany

²Fachbereich Physik, Universität Osnabrück, D-49076 Osnabrück

(Dated: September 22, 2020)

The presence of flat bands is a source of localization in lattice systems. While flat bands are often unstable with respect to interactions between the particles, they can persist in certain cases. We consider a diamond ladder with transverse hopping that possesses such stable flat bands and show that many-body localization appears in the presence of interactions. We demonstrate that the eigenstate thermalization hypothesis is violated and verify localization by time evolution of local observables, revival probabilities, and participation ratios. Thus, this system appears to be an example for many-body localization without disorder.

Many-body localization (MBL) is usually seen as a generalization of Anderson localization to interacting systems and thus is discussed to occur in disordered systems [1, 2]. These systems do not thermalize even in the presence of an interaction between the particles. Systems that exhibit MBL have been studied both theoretically and experimentally, because they can retain some memory of the initial conditions and are thus of interest for storing quantum information [1–3] and hence may implement quantum memory devices. However, disorder breaks the translational invariance of these systems. There has been a discussion whether MBL could also exist in systems without disorder [4–13]. Recently, flat band systems have been considered in this context [13–16]. Noninteracting flat band systems are characterized by the presence of flat energy dispersions and thus possess highly degenerate energy eigenstates. This in turn allows localized stationary eigenstates in the system. As a result, the flat band is a different source of localization in these systems and could equally well (instead of Anderson localization) lead to interacting many-body quantum systems that possess localization in the presence of particle-particle interactions. Flat bands are often unstable against interaction, though [17]. However, there exist specific models where flat bands can survive in presence of interaction due to symmetry protection [18] or in detangled systems [16], for example. Here, we study the one-dimensional diamond ladder [Fig. 1(a)] for spinless fermions, which previously was shown to host such stable flat bands [18]. The question of thermalization is closely related to the so-called eigenstate thermalization hypothesis (ETH) [19–21], which postulates that every energy eigenstate yields expectation values close to the corresponding microcanonical values. MBL systems have been found to violate ETH, see e.g. [1, 22]. We will provide evidence for MBL in the one-dimensional diamond ladder by showing that the ETH is violated in this system. We support our results by an analysis of the time evolution of the revival probability and the participation ratio for nonequilibrium initial states, quantities that characterize localization in many-body quantum systems [23–25].

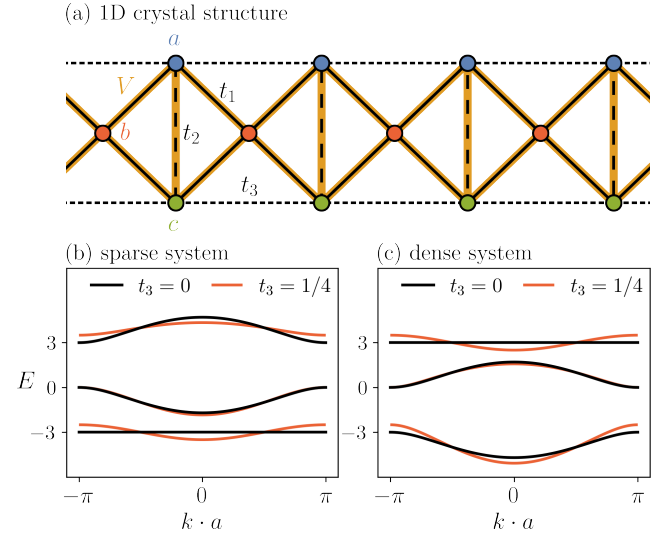


FIG. 1. Quasi one-dimensional lattice (diamond ladder) with periodic boundaries containing flat bands. (a) Crystal structure with three orbitals a , b , c per unit cell and three kinds of hoppings t_1 (solid), t_2 (dashed) and t_3 (dotted). V represents particle-particle interaction along solid and dashed lines. (b) Single-particle band structure (black) for the sparse system ($t_2 = -3$). The flat band lies below the other two bands and may be made dispersive for $t_3 \neq 0$ (red). (c) Same for the dense system ($t_2 = +3$). The flat band lies above the other bands.

The Hamiltonian of the system reads:

$$H = - \sum_{\langle i\alpha, j\beta \rangle} t_{i\alpha, j\beta} \cdot c_{j\beta}^\dagger c_{i\alpha} + \frac{V}{2} \sum_{\langle\langle i\alpha, j\beta \rangle\rangle} n_{j\beta} n_{i\alpha}, \quad (1)$$

with fermionic creation (annihilation) operators $c_{i\alpha}^\dagger$ ($c_{i\alpha}$) in unit cell i for the orbital $\alpha \in \{a, b, c\}$ and particle density operators $n_{i\alpha} = c_{i\alpha}^\dagger c_{i\alpha}$. $t_{ia, jb} = t_{ic, jb} = t_1$ describes nearest-neighbor hopping, $t_{ia, ic} = t_2$ stands for next-nearest-neighbor hopping within same unit cells, and $t_{ia, i\pm 1a} = t_{ic, i\pm 1c} = t_3$ permits hopping to next-nearest neighbors of adjacent cells as illustrated in Fig. 1(a). In the following we will choose

t_1 as the unit of energy and thus set $t_1 = 1$. V indicates (next-)nearest-neighbor repulsive particle-particle interaction. $\langle i\alpha, j\beta \rangle$ stands for a summation over all nearest- and next-nearest-neighbored lattice sites i and j with orbitals α and β along all types of lines in Fig. 1(a). $\langle\langle i\alpha, j\beta \rangle\rangle$ omits summation over dotted lines. Thus, the interaction only acts on the original diamond ladder structure. The transversal hopping amplitude $t_2 = \pm 3$ determines whether the flat band lies below or above the other bands [see Fig. 1(b) and (c)]. Throughout this work we focus on the case where the flat band is half filled. For $t_2 = -3$ the system is thus 1/6-filled and we denote this as sparse system. For $t_2 = 3$, on the other hand, the system is 5/6-filled and we denote this as dense system. We have introduced the inter-cell hopping t_3 , because it allows to purposely turn on a dispersion of the flat bands. Below, we will discuss the case $t_3 = 1/4$ [see red curves in Fig. 1(b) and (c)] as a comparison system without flat bands. In a previous work we have shown that the flat bands in this system are robust with respect to the particle-particle interaction unless V becomes larger than approximately 1.8 [18]. Also, the many-particle ground state remains macroscopically degenerate for finite $V \lesssim 1.8$.

As a first step to assess whether this interacting system shows MBL, we numerically test if the ETH is broken or not. In a system that thermalizes one expects that expectation values of observables $\langle A \rangle$ in energy eigenstates with similar energy do not fluctuate much from one eigenstate to another. If a system possesses stationary and localized states, however, we expect the ETH to be broken. Then, the states possess local information which leads to an higher amount of fluctuations of $\langle A \rangle$. In the thermodynamic limit these fluctuations will remain finite, while they will go to zero, when ETH is fulfilled.

To test ETH numerically, we use the method of Ref. [26] which is based on an accurate scheme based on typical pure states drawn at random [27]. An energy filter around energy U with width σ is applied on a Gaussian distributed (mean zero) normalized random state $|\Psi\rangle$:

$$|\Phi\rangle = \exp\left[-\frac{(H-U)^2}{4\sigma^2}\right] \cdot |\Psi\rangle. \quad (2)$$

We chose U to be equal to the ground-state energy and a small $\sigma = 3/2$. $|\Phi\rangle$ then contains ground states and a mix of energetically low-lying excited states. The quantity

$$\Sigma = \sqrt{\frac{\{\int_t \langle \Phi | A(t) A | \Phi \rangle\}}{\{\langle \Phi | \Phi \rangle\}} - \frac{\{\langle \Phi | A | \Phi \rangle\}^2}{\{\langle \Phi | \Phi \rangle\}^2}} \quad (3)$$

measures fluctuations of the expectation values of A . Here, the curly brackets indicate that these values are averaged over different random states $|\Psi\rangle$. The time average is $\int_t = 1/(t_e - t_i) \int_{t_i}^{t_e} dt$ where t_i and t_e are suitably

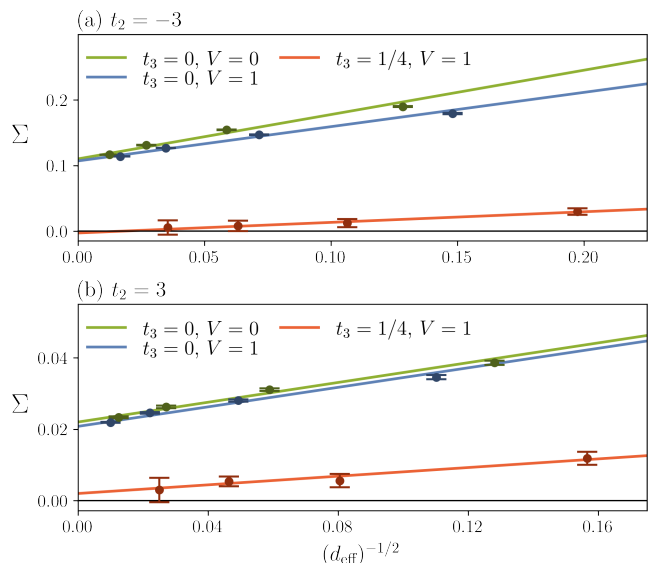


FIG. 2. Results of the ETH calculations. (a) Decrease of expectation value fluctuations with increasing system size for the sparse system. Σ only tends to zero if $t_3 \neq 0$ and the flat band becomes dispersive. (b) Corresponding results for the dense system. Error bars show the statistical error coming from the average over a finite number of random states $|\Psi\rangle$.

chosen such that the integral best matches the relaxation value of $\langle \Phi | A(t) A | \Phi \rangle$ [26]. The first fraction therefore serves as long-term auto correlation. The second term is simply the squared expectation value of A in the filtered state. Its square root is a good estimate of the actual ensemble average. Deviations between the first and second term will typically become smaller when the system size is increased. They will go to zero if the states thermalize. However, if the system breaks ergodicity and preserves information of the initial state over long times, the fluctuations will not vanish and Σ will take a finite value.

For the operator A we choose:

$$A = \frac{N}{M(N-1)} \sum_{i\alpha} \sin^2\left(\frac{(i-1) \cdot \pi}{N-1}\right) \cdot n_{i\alpha}. \quad (4)$$

N is the number of unit cells and M is the number of particles. This quantity detects particle density inhomogeneities along the lattice. For homogeneously distributed states the expectation value is $1/2$.

In Fig. 2 we present our results for the sparse and dense system with different system sizes. Each regression line contains four points for $N = 6, 8, 10, 12$ unit cells and $M = 3, 4, 5, 6$ particles in the sparse and $M = 15, 20, 25, 30$ particles in the dense setting. The Hilbert space dimension is $d = \binom{3 \cdot N}{M}$ and ranges from 816 to 1.9 million. The effective dimension d_{eff} that is probed by the state $|\Phi\rangle$ is calculated from:

$$d_{\text{eff}} = d \cdot \{\langle \Phi | \Phi \rangle\}. \quad (5)$$

Matrix exponentials in (2) and (3) are performed via Krylov subspace algorithms [28, 29]. We have chosen the interaction strength $V = 1$ in order to stay below the critical value of ≈ 1.8 [18].

For the dispersive system ($t_3 = 1/4$) the fluctuations scale with the inverse square root of the effective dimension, which one should expect for generic nonintegrable systems [30]. In contrast, if the flat band is present ($t_3 = 0$), the fluctuations do not vanish in the limit $d_{\text{eff}} \rightarrow \infty$ both with and without interactions. This observation holds for both the sparse and the dense system, while in the latter case the fluctuations are one order of magnitude smaller. Only if we turn on the dispersion, the system shows thermalization. This is one of our central results, as it shows that ETH remains violated also in the presence of interaction.

Next, we take a look at the time evolution of selected initial nonequilibrium states and examine the influence of the flat band. As the initial states we choose the real-space eigenstates depicted in Fig. 3(a), $|\Psi_s^{10}\rangle$ for the sparse system and $|\Psi_d^{10}\rangle$ for the dense system. They are characterized by an asymmetric accumulation of particles (holes) in the center of the chain. They are defined by

$$|\Psi_{s,d}^{10}\rangle = \left(\prod_{i\alpha}^{\text{occ}} c_{i\alpha}^\dagger \right) |0\rangle \quad (6)$$

where $|0\rangle$ is the vacuum state and the product runs over the occupied sites (black circles) in Fig. 3(a). The system sizes are 10 unit cells with 5 and 25 particles, respectively, yielding a Hilbert-space dimension of $d = 142506$ for both cases. Starting with these configurations, we calculate the time evolution numerically and consider three different quantities which provide information on localization over time [24, 25]. The results in Fig. 3(b) show the expectation values of the inhomogeneity operator (4) measured for $|\Psi_{s,d}^{10}(t)\rangle$. The initial value $\langle A(0) \rangle$ has to be equal for same initial states, however, the time evolution is strongly influenced by the value of t_3 . For $t_3 \neq 0$ the expectation values approach $\langle A \rangle_{\text{eq}} = 1/2$ corresponding to thermal equilibrium and only vary weakly from then on. If the band is flat for $t_3 = 0$, the relaxation values stay at $\langle A \rangle_\infty \approx 0.784$ for the sparse and $\langle A \rangle_\infty \approx 0.441$ for the dense system, showing that the system retains a memory of the initial state.

In Fig. 3(c) we show the revival probabilities $R(t) = |\langle \Psi_{s,d}^{10}(t) | \Psi_{s,d}^{10} \rangle|^2$ which give the probabilities for evolving states to return back into their initial settings. In the flat-band case the revival probability approaches a much larger value R_∞ for long times around which $R(t)$ fluctuates. The ratio between R_∞ for $t_3 = 0$ and $t_3 = 1/4$ is 27.59 in the sparse and 37.36 in dense case. Hence, it is in both cases many times more probable to return if the flat band is present, again showing a higher degree of localization.

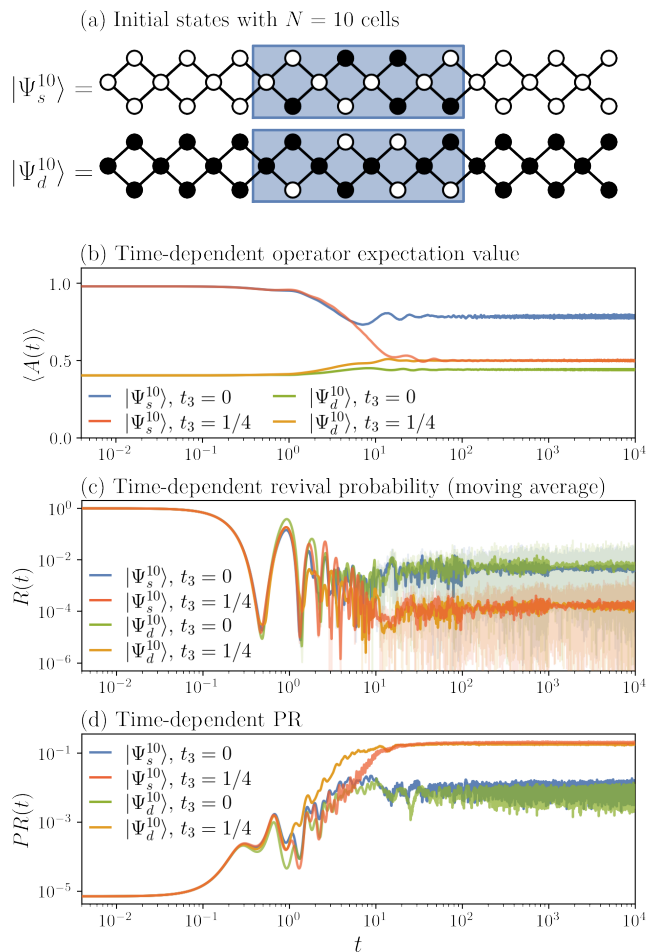


FIG. 3. Time evolution with interaction $V = 1$ for a system with 10 unit cells on a logarithmic time scale. (a) $|\Psi_s^{10}\rangle$ and $|\Psi_d^{10}\rangle$ in real space representation are the initial states for the sparse and dense system, respectively. (b) The evolution of inhomogeneity in terms of the operator A . (c) Probability for the evolved state to return into its initial condition. Due to strong fluctuations, we show the moving average (intense color) above the original data (light color). (d) Evolution of the participation ratio as measure for localization.

In Fig. 3(d) the time evolution of the participation ratio (PR) is shown. It is defined as [23, 24]:

$$PR(t) = \left[d \sum_{i=1}^d |\langle \Psi_{s,d}^{10}(t) | \chi_i \rangle|^4 \right]^{-1}, \quad (7)$$

with $|\chi_i\rangle$ being the real-space many-particle basis. The participation ratio is a measure of how strongly a many-particle state is distributed over the real-space basis. Possible values range from $1/d$ for a maximally localized state to 1 for full de-localization. Again, we can observe that the states in the system with flat band tend to be significantly more localized at long times than without flat band. Ratios of the long-time participation ratios PR_∞ between $t_3 = 1/4$ and $t_3 = 0$ are 22.20 (sparse)

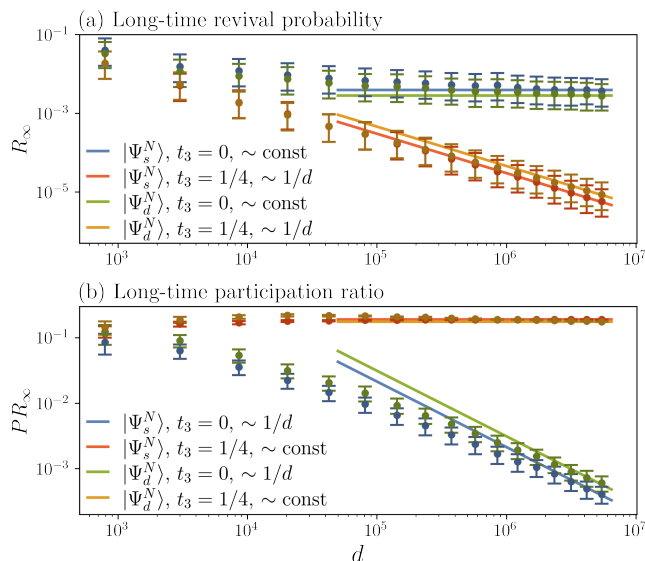


FIG. 4. Long-time values R_∞ and PR_∞ vs. Hilbert space dimension d . The system sizes are from 12 to 60 lattice sites with either 5 particles or 5 holes. The Hilbert-space dimension varies between $d = 792$ and $d = 5461512$. Regression lines are fitted to the largest dimensions. Error bars show the amount of fluctuation around the long-time value.

and 28.34 (dense).

To judge more clearly the localization, it is of interest to study the dependence of the long-time values R_∞ and PR_∞ on the system size. To do so, we calculate them by removing or adding more unit cells to the system. The initial states $|\Psi_{s,d}^N\rangle$ are generalized for chains of different length. The smallest systems possess $N = 4$ unit cells, i.e. 12 lattice sites with 5 particles (sparse system) and 7 particles (dense system) which contain only the four cells in the center shown as the blue area in Fig. 3(a). Then, we add empty (sparse) or filled (dense) cells step by step up to $N = 20$, i.e. up to 60 lattice sites with either 5 or 55 particles. In the limit of large chains, R_∞ should be independent of the Hilbert-space dimension d if the system is many-body localized and proportional to d^{-1} if it is not. Due to the factor d in (7), the opposite holds for PR_∞ . The results in Fig. 4 show that for large Hilbert-space dimensions in the flat band case ($t_3 = 0$) R_∞ remains constant, while PR_∞ decreases like d^{-1} , which one expects for a many-body localized system. In contrast, for $t_3 = 1/4$ the revival probability R_∞ decreases like d^{-1} and PR_∞ remains constant, indicative for an ergodic system.

The initial states in Fig. 3(a) have energies that lie approximately in the center of the energy spectrum of the Hamiltonian and thus provide information in that energy range. It is of interest to also look at the characteristics of the PR over the full spectrum of the Hamiltonian along the lines of Ref. [23]. In Fig. 5 we show the PR for the whole spectrum of eigenstates for a system of 8 unit cells

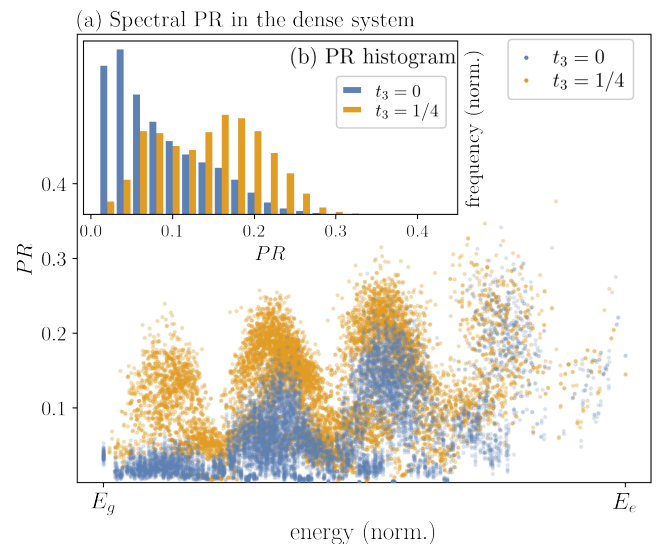


FIG. 5. Full spectrum localization properties with interaction $V = 1$ and a system size of 24 sites with 20 particles. (a) Participation ratio for all energy eigenstates with and without flat band. The energy levels are normalized to the width of the spectrum. E_g is the ground state energy and E_e the energy of the highest excited state. (b) Histogram corresponding to the values of (a).

with 20 particles (4 holes, a dense system). Here, the Hilbert-space dimension is $d = 10626$, allowing us to determine all eigenstates by exact diagonalization. Within the degenerate subspaces we generate random superpositions to obtain a set of representative PR values for each distinct energy level. From Fig. 5(a) it can be seen that the PR is larger for $t_3 = 1/4$ than for $t_3 = 0$ almost over the whole spectrum. Differences are largest at low energies and become smaller for higher energies. In Fig. 5(b) a histogram of the number of PR values is shown, which demonstrates that the flat-band system possesses a larger number of low-PR-value energy states than the dispersive system.

To summarize, we examined quasi one-dimensional interacting diamond ladders which provide flat bands. The configurations were chosen to model four cases: sparse filling with and without flat band and dense filling with and without flat band. The flatness was controlled via an inter-cell hopping parameter. We have shown that the flat band cases violate the eigenstate thermalization hypothesis. Time dependence of selected nonequilibrium initial states showed that the system retains a memory of the initial state. Finite-size scaling of the revival probability and participation ratio was shown to be consistent with localization. An analysis of the full spectrum of eigenstates showed that localization is strongest for lower energies and gradually increases for higher energy states. Taken together, our results reliably show that this system provides an example for many-body localization in

a defect-free flat-band system.

Financial support from the DFG via the research group FOR2692, grant numbers 397171440 and 397067869 is gratefully acknowledged. We would like to thank S. kleine Brüning and S. Tilleke for valuable discussions.

* thomas.dahm@uni-bielefeld.de

- [1] R. Nandkishore and D. A. Huse, *Annual Review of Condensed Matter Physics* **6**, 15 (2015).
- [2] D. A. Abanin, E. Altman, I. Bloch, and M. Serbyn, *Rev. Mod. Phys.* **91**, 021001 (2019).
- [3] M. Schreiber *et al.*, *Science* **349**, 842 (2015).
- [4] Z. Papic, E. M. Stoudenmire, and D. A. Abanin, *Annals of Physics* **362**, 714 (2015).
- [5] N. Y. Yao, C. R. Laumann, J. I. Cirac, M. D. Lukin, and J. E. Moore, *Phys. Rev. Lett.* **117**, 240601 (2016).
- [6] A. Smith, J. Knolle, D. L. Kovrizhin, and R. Moessner, *Phys. Rev. Lett.* **118**, 266601 (2017).
- [7] M. Brenes, M. Dalmonte, M. Heyl, and A. Scardicchio, *Phys. Rev. Lett.* **120**, 030601 (2018).
- [8] Z. Lan, M. van Horssen, S. Powell, and J. P. Garrahan, *Phys. Rev. Lett.* **121**, 040603 (2018).
- [9] E. van Nieuwenburg, Y. Baum, and G. Refael, *Proceedings of the National Academy of Sciences* **116**, 9269 (2019).
- [10] P. P. Mazza, G. Peretto, A. Lerose, M. Collura, and A. Gambassi, *Phys. Rev. B* **99**, 180302 (2019).
- [11] J. Sirker, *Phys. Rev. B* **99**, 075162 (2019).
- [12] T. Heitmann, J. Richter, T. Dahm, and R. Steinigeweg, *Phys. Rev. B* **102**, 045137 (2020).
- [13] P. A. McClarty, M. Haque, A. Sen, and J. Richter, preprint, arXiv:2007.01311 (2020).
- [14] Y. Kuno, T. Orito, and I. Ichinose, *New Journal of Physics* **22**, 013032 (2020).
- [15] N. Roy, A. Ramachandran, and A. Sharma, preprint, arXiv:1912.09951 (2019).
- [16] C. Danieli, A. Andreanov, and S. Flach, *Phys. Rev. B* **102**, 041116 (2020).
- [17] D. Leykam, A. Andreanov, and S. Flach, *Advances in Physics: X* **3**, 1473052 (2018).
- [18] S. Tilleke, M. Daumann, and T. Dahm, *Z. Naturforsch. A.* **75**, 393 (2020).
- [19] J. M. Deutsch, *Phys. Rev. A* **43**, 2046 (1991).
- [20] M. Srednicki, *Phys. Rev. E* **50**, 888 (1994).
- [21] M. Rigol, V. Dunjko, and M. Olshanii, *Nature* **452**, 854 (2008).
- [22] A. Pal and D. A. Huse, *Phys. Rev. B* **82**, 174411 (2010).
- [23] W. Beugeling, A. Andreanov, and M. Haque, *Journal of Statistical Mechanics: Theory and Experiment* **2015**, P02002 (2015).
- [24] E. J. Torres-Herrera and L. F. Santos, *Annalen der Physik* **529**, 1600284 (2017).
- [25] M. Schiulaz, E. J. Torres-Herrera, F. Pérez-Bernal, and L. F. Santos, *Phys. Rev. B* **101**, 174312 (2020).
- [26] R. Steinigeweg, A. Khodja, H. Niemeyer, C. Gogolin, and J. Gemmer, *Phys. Rev. Lett.* **112**, 130403 (2014).
- [27] For other applications of random states see T. Heitmann, J. Richter, D. Schubert, and R. Steinigeweg, *Z. Naturforsch. A.* **75**, 421 (2020).
- [28] C. Moler and C. Loan, *Society for Industrial and Applied Mathematics* **45**, 3 (2003).
- [29] N. Mohankumar and S. M. Auerbach, *Computer Physics Communications* **175**, 473 (2006).
- [30] W. Beugeling, R. Moessner, and M. Haque, *Phys. Rev. E* **89**, 042112 (2014).